Single-cell analyses reveal increased gene expression variability in human neurodevelopmental conditions

Graphical abstract

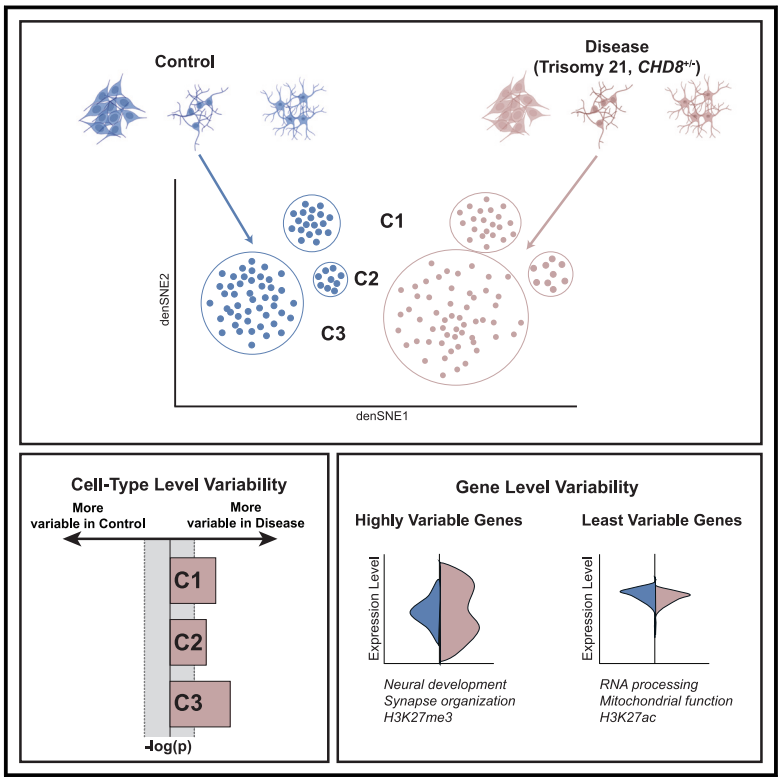

Authors

Suraj Upadhya, Jenny A. Klein, Anna Nathanson, Kristina M. Holton, Lindy E. Barrett

Correspondence

lbarrett@broadinstitute.org

This study investigates gene expression variability in human neurodevelopmental conditions. Using single-cell analyses of brain cell types, we identify a significant increase in gene expression variability driven by trisomy 21 as well as *CHD8* haploinsufficiency. Additional analyses ascertain core features of highly and least variable genes across independent datasets.

Upadhya et al., 2025, The American Journal of Human Genetics *112*, 876–891
April 3, 2025
https://doi.org/10.1016/j.ajhg.2025.02.011

CellPress

ARTICLE

Single-cell analyses reveal increased gene expression variability in human neurodevelopmental conditions

Suraj Upadhya,[1,2] Jenny A. Klein,[1,2] Anna Nathanson,[1,2] Kristina M. Holton,[1,2] and Lindy E. Barrett[1,2,*]

Summary

Interindividual variation in phenotypic penetrance and severity is found in many neurodevelopmental conditions, although the underlying mechanisms remain largely unresolved. Within individuals, homogeneous cell types (i.e., genetically identical and in similar environments) can differ in molecule abundance. Here, we investigate the hypothesis that neurodevelopmental conditions can drive increased variability in gene expression, not just differential gene expression. Leveraging independent single-cell and single-nucleus RNA sequencing datasets derived from human brain-relevant cell and tissue types, we identify a significant increase in gene expression variability driven by the autosomal aneuploidy trisomy 21 (T21) as well as autism-associated chromodomain helicase DNA binding protein 8 (*CHD8*) haploinsufficiency. Our analyses are consistent with a global and, in part, stochastic increase in variability, which is uncoupled from changes in transcript abundance. Highly variable genes tend to be cell-type specific with modest enrichment for repressive H3K27me3, while least variable genes are more likely to be constrained and associated with active histone marks. Our results indicate that human neurodevelopmental conditions can drive increased gene expression variability in brain cell types, with the potential to contribute to diverse phenotypic outcomes. These findings also provide a scaffold for understanding variability in disease, essential for deeper insights into genotype-phenotype relationships.

Introduction

Questions around inter- and intra-individual variation in development, aging, and disease are of high basic and clinical relevance. Trisomy 21 (T21) is the most common genetic cause of intellectual disability, affecting around 6 million individuals globally. While T21 is the most viable autosomal trisomy, rates of spontaneous prenatal loss are high, indicating that T21 is not invariably compatible with postnatal viability.[1,2] For individuals born with T21, there is a core set of neurological and non-neurological phenotypes, in addition to >80 potential co-occurring conditions associated with but not specific to the condition, including childhood leukemia, epilepsy, early-onset Alzheimer disease, and congenital heart disease.[1] The incomplete penetrance and variable severity of most phenotypes is striking given that T21 occurs *de novo*, most commonly due to errors in maternal meiosis.[2,3]

There is a critical gap in our understanding of the mechanisms driving phenotypic variation. In the case of T21, variation is often attributed to allelic differences either on or off chromosome 21 (HSA21) and/or to physical or social environmental factors. Notably, studies in yeast found that aneuploidy itself was sufficient to increase non-genetic phenotypic variability.[4,5] By introducing chromosome gains and losses into isogenic budding yeast, Beach et al. quantified increased variability in cell cycle kinetics, gene expression, and response to perturbations, theorizing that gene-dosage disruptions reduced the fidelity of biological systems.[4] Another study assessing the impact of antifungal or chemotherapeutic drugs in budding yeast also found significant phenotypic variability among clones in response to aneuploidy.[5] The hypothesis that autosomal aneuploidies like T21 could drive increased variability in complex multicellular systems has not been systematically investigated. Moreover, while variability in molecular expression has well-documented functional roles in development, aging, and cancer, the concept remains almost entirely unexplored in the context of neurodevelopmental conditions.

Cell-to-cell variability in otherwise homogeneous cell types may be driven by intrinsic or extrinsic factors, also referred to as stochastic and deterministic, respectively. Stochasticity is found in diverse biological processes, including X chromosome inactivation and olfactory receptor choice.[6] Stochasticity in molecular expression may be influenced by the fundamental randomness of biochemical reactions governing transcription, RNA processing, translation, and degradation[7]; limited expression levels of regulatory molecules; transcriptional bursting; and/or random partitioning of molecules during cell division.[8] Extrinsic factors, such as differences in microenvironment or cell size, can also drive variability.[8–11] While sometimes referred to as "noise" in the context of RNA sequencing, variability in transcript abundance can encode meaningful information.[12] For example, variability in molecular expression as early as the 4-cell stage of mouse embryos has been shown to alter cell fate,[13] and varying levels of

[1]Stanley Center for Psychiatric Research, Broad Institute of MIT and Harvard, Cambridge, MA 02142, USA; [2]Department of Stem Cell and Regenerative Biology, Harvard University, Cambridge, MA 02138, USA
*Correspondence: lbarrett@broadinstitute.org
https://doi.org/10.1016/j.ajhg.2025.02.011.

Sca-1 in mouse hematopoietic progenitor cells have been shown to impact differentiation to erythroid or myeloid lineages.[14] In the context of disease, variability in protein levels in cancer cell lines led to differences in TRAIL (tumor necrosis factor-related apoptosis-inducing ligand)-mediated apoptosis.[15] Single-cell analyses have further revealed that upon drug treatment, diverse cancer cell clones can emerge harboring functional and gene expression differences, with no evidence for genomic mutations.[16] Increased gene expression variability is also correlated with organismal aging[17,18]; mechanistically, the speed of transcriptional elongation has been shown to increase with age, which can, in turn, impact the fidelity of transcriptional processing.[19] Our understanding of biological variability, whether driven by intrinsic or extrinsic factors, thus has important implications for human development, aging, and disease.

To test the hypothesis that human neurodevelopmental conditions may drive increased variability in gene expression, not just differential gene expression, we performed systematic analyses of both new and published single-cell and single-nucleus RNA sequencing (scRNA-seq and snRNA-seq) datasets derived from brain-relevant cell and tissue types. We identified a significant increase in gene expression variability driven by T21 in three independent datasets, including in human neural progenitor cells (NPCs) and postmortem human brain tissue compared with euploid controls. Differential variability was uncoupled from differential expression, and decreased gene-gene correlation strength in some T21 datasets was consistent with stochastic changes. Analyses of syndromic autism models also revealed increased gene expression variability driven by the loss of the high-confidence autism-associated gene chromodomain helicase DNA binding protein 8 (*CHD8*) in human brain organoid models, indicating that these findings are not restricted to autosomal aneuploidy. We then leveraged these scRNA-seq and snRNA-seq datasets to ascertain core features of highly and least variable genes (HVGs and LVGs, respectively), with LVGs enriched for non-cell-type-specific functions, active chromatin marks, and a set of transcription factor (TF) motifs, in contrast to HVGs, which were largely cell-type specific with modest enrichment for H3K27me3 and no identifiable TF signature. Collectively, our analyses reveal increased variability in gene expression within brain-relevant cell and tissue types from two neurodevelopmental conditions, with the potential to influence phenotypic outcomes.

Material and methods

Cell culture

All experiments performed using human induced pluripotent stem cells (iPSCs) followed institutional review board (IRB) guidelines approved by Harvard University. Isogenic human iPSC lines were purchased from WiCell (T21 line: DS1, euploid line: DS2U). iPSCs were grown in mTeSR+ (STEMCELL Technologies) on Geltrex-coated plates and passaged with TrypLE (Thermo Fisher Scientific) plus ROCKi. iPSCs were induced into NPCs using the STEMDiff SMADi Neural Induction Kit (STEMCELL Technologies). NPCs were grown in 6-well plates, with 3 wells per genotype. Media was changed daily, and Accutase was used to passage cells following the initial induction. After 3 weeks, NPCs were transferred to STEMDiff neural progenitor medium (STEMCELL Technologies) for one additional week, after which the cells were collected for scRNA-seq analysis. All cells were grown in a 5% CO_2 and 37°C incubator and tested monthly for mycoplasma contamination. G-banding karyotype analysis was used to confirm the expected chromosome counts (Cell Line Genetics).

scRNA-seq

Three wells of NPCs per genotype were pooled together to obtain 1–1.5 million cells for scRNA-seq cell preparation following instructions from Illumina. The cDNA library was made using the 10× Genomics Chromium Single Cell 3′ Library and Bead Kit v.3. Sequencing was performed on the NovaSeq 6000 by the Bauer Core Facility at Harvard University. The T21 sample had 1,472,632,952 reads with 133,463 mean reads per cell. The euploid sample had 1,054,149,472 reads with 120,035 mean reads per cell. Paired-end-read FASTQ files were aligned to GRCh38 Genome Reference Consortium Human Reference 38 (hg38) using the "count" method of Cell Ranger v.8.0.1.4.[20]

scRNA-seq analysis

Cell Ranger output files, filtered barcodes, features, and matrix files from Qiu et al.[21] were retrieved from the Gene Expression Omnibus (GEO: GSE208625). FASTQ files from Palmer et al.[22] were accessed through the European Genome-Phenome Archive through accession number EGAS00001005691 in agreement with the Chun lab Data Access Committee. Paulsen et al.[23] Seurat objects were retrieved from Synapse (projectID: syn26346373). FASTQ files from Villa et al.[24] were obtained from ArrayExpress (accession: E-MTAB-11406). Published scRNA-seq datasets Qiu et al.,[21] Palmer et al.,[22] and Villa et al.[24] were retrieved and reanalyzed using Seurat v.5 (5.0.0) in R (4.2.1).[25–27] Paulsen et al.[23] data were not reprocessed using Seurat v.5, as we employed the clustering analysis provided with their data. Analysis was performed independently for each dataset. SCTransform was first used to normalize each sample individually.[26] DoubletFinder (2.0.4) was performed where non-aggregated data were retrieved.[28] The pK parameter was set to the maximum of the bimodality coefficient distribution. The homotypic doublet proportion estimate was calculated using the 10× Genomics multiplet rate per cells recovered (Chromium Single Cell V(D)J Reagent Kits with feature barcoding technology for cell surface protein, document no. CG000186 Rev A, 10× Genomics [July 25, 2019]). For our dataset, we set the T21 and euploid samples' multiplet rate to 8% and 6.5%, respectively. All samples were then merged. Subsequently, the CellCycleScoring function was used to annotate cell cycle effects, which were regressed out in a subsequent call for SCTransform. Principal-component analysis (PCA) was done on the Pearson residuals output from SCTransform. Data were then integrated using the canonical correlation analysis (CCA), recpirpocal PCA (RPCA), and Harmony methods.[25,29] For each integration method, the top 30 components were then used for uniform manifold approximation and projection (UMAP). Clusters were then identified with FindNeighbors and FindClusters. Based on

the integration results and clustering, the preferred integration method and clustering for each dataset was chosen for subsequent analysis. We used CCA for our data and the Qiu et al.[21] and Villa et al.[24] datasets. We used Harmony for the Palmer et al.[22] data.

Differential gene expression and differential variability analysis

Differential gene expression analysis was performed for select clusters to assess the correlations of differential expression and differential variability in our dataset and illustrate differential gene expression statistics for example HVGs and LVGs from our data and the Qiu et al.,[21] Palmer et al.,[22] and Paulsen et al.[23] datasets. For our dataset, we performed differential expression analysis on the uncommitted progenitor clusters: progenitor 1, cycling progenitor, and progenitor 2. We performed differential gene expression analysis on progenitor 3 from Qiu et al.,[21] the most variable astrocyte cluster from Palmer et al.,[22] and the most variable callosal projection neuron (CPN) cluster from the CHD8_GM_3m_r1 organoid from Paulsen et al.[23] We used the FindMarkers function from Seurat v.5 to perform differential gene expression analysis, using the Wilcoxon rank-sum test[30] to determine statistical significance. We set the min.pct parameter to 0.25 to include only genes expressed in 25% of cells in either group, comparing the conditions for each cluster independently. In our data, we further calculated the differential variability, the difference between T21 residual and euploid residual for each gene, in our three progenitor clusters. We illustrated the relationship between differential gene expression and differential variability using ggplot2 (3.5.0), displaying the Pearson correlation coefficient of the fitted linear model calculated using the geom_smooth function.[31]

Cell type variability

Following cell type annotation of each UMAP-derived cluster, published methods were used to characterize cell types that were differentially variable between disease and control.[32] Briefly, the method detailed by Liu et al.[32] implements a distance metric to quantify variability. The data are normalized by the Seurat v.5 native function NormalizeData using the relative counts method for normalization. Subsequently, all genes are used to calculate 200 PCA components. A density-preserving stochastic neighbor embedding (denSNE) was then calculated using the 200 PCs.[33] Compared to t-distributed SNE (tSNE), denSNE was found to maintain the local density of clusters. Using the denSNE coordinates, the medoid, or the cell with the least distance to all other cells in the cell type cluster, was found for each cell type. Each cell's distance to the medoid was then calculated for each cell type using the pairwise_distances function from the sklearn (1.0.2) Python (3.9.12) package.[34] The two-sided Wilcoxon rank-sum test was performed to evaluate significant differences in mean distance to the medoid between the disease and wild type (WT), followed by Benjamini-Hochberg correction for multiple comparisons.[35] We used the function ranksums from the Python SciPy package (1.9.3) to calculate the Wilcoxon rank-sum test and the fdrcorrection function from the Python statsmodel (0.14.0) package for p value correction.[36,37] An alpha threshold of 0.05 was set to evaluate statistical significance.

Gene-level variability

Gene-level variability was evaluated for each cluster independently. Within each cluster, only genes that were expressed in at least 5% of cells were kept for further analysis. The method developed by Brennecke et al. and employed by Osorio et al. and Cai was used to ascertain variable genes.[38–40] Normalized counts were calculated using DESeq2's estimateSizeFactors function, followed by the counts function with the normalized parameter set to "true." This normalization method implements the median ratios method, which accounts for RNA sequencing depth and composition.[41] The poscounts method was used for estimateSizeFactors because some samples had genes with few zeros and this method employs an alternative geometric mean calculation to allow for some zeros to calculate the median ratios.[41] Subsequently, a general linear model (GLM) was fitted on genes that met the mean threshold using the linear_model, LinearRegression, and fit functions from the Python sklearn package (1.0.2).[34] This threshold was defined such that only 5% of genes with a squared coefficient of variation (CV^2) greater than 0.3 would surpass the mean threshold. This served to limit the effect of high CV^2 genes on the fit. Equation 1 illustrates the relationship between mean expression (μ) and expected CV^2 (CV^2_{exp}), where the coefficients alpha$_1$ (a_1) and a_0 are found after fitting the data. The GLM fit accounted for technical noise.

$$CV^2_{exp} \approx a_1 \Big/ \mu + a_0 \qquad \text{(Equation 1)}$$

The residual (CV^2_{obs}/CV^2_{exp}) was then used to determine significant variability. Brennecke et al.[38] described the use of a one-sided test, with the assumption that the residual sampling distribution is that of a $\chi 2$ distribution, with degrees of freedom being the number of cells minus 1. Equation 2 displays this relationship with the GLM equation in place of CV^2_{exp}.

$$\frac{CV^2_{obs}}{a_1/\mu + a_0} \sim \chi^2_{m-1} \Big/ (m-1) \qquad \text{(Equation 2)}$$

To evaluate both HVGs and LVGs, a two-sided test was implemented using the same sampling distribution assumption as Brennecke et al.[38] We used the chi2.cdf function from the Python SciPy package (1.9.3) to determine p values from the $\chi 2$ distribution.[36] After this, p values were corrected for multiple comparisons using the Benjamini-Hochberg method with the fdrcorrection function from the Python statsmodel (0.14.0) package.[37] An alpha threshold of 0.05 was set to evaluate statistical significance.

GO analysis of HVGs and HVGs

For each dataset, the top three clusters presenting with increased variability in the disease state compared to the common cell type were selected for Gene Ontology (GO) analysis. First, thresholds of 1.1 for HVGs and 0.9 for LVGs were set for the residuals. For GO analysis, we implemented less stringent criteria for gene selection to assess an overall impact on biological pathways. All the genes between the selected clusters per dataset were collected and used for analysis by the clusterProfiler R package (4.4.4).[42] For our data, we evaluated the HVGs and LVGs from the clusters progenitor 1, cycling progenitor, and progenitor 2. From the Qiu et al.[21] data, we analyzed genes from progenitor 1, progenitor 2, and progenitor 3. The three most variable oligodendrocyte clusters, CPN clusters, and excitatory neuron clusters from Palmer et al.,[22] Paulsen et al.'s[23] CHD8_GM_3m_r1 organoid, and Villa et al.'s[24] 120-day organoid datasets, respectively, were analyzed. The compareCluster function from clusterProfiler was utilized to compare both control and disease states as well as HVGs and LVGs. The simplify function was used to reduce redundant terms.

Constraint analysis

We employed more stringent selection criteria for genes to be used for the constraint analysis to limit the impact of low expressed genes and small residual deviations on the analysis. Thus, we selected the top 150 HVGs with the greatest residuals and the top 150 LVGs with the smallest residuals that met a mean-normalized gene expression cutoff of 0.70. The normalization used was that of DESeq2, which implements the median of ratios method,[41] to remain consistent with the gene-level variability analysis. The constraint metrics from the genome aggregation database (gnomAD v.4.1.0) were used to further characterize the HVGs and LVGs.[43] The LOEUF (loss-of-function observed/expected upper bound fraction) metric of the 150 genes meeting the expression threshold was used to assess each gene's constraint. The two-sided Wilcoxon test, as implemented by the wilcox_test function from the rstatix (0.7.2) package in R, was employed to determine significant differences between LVGs and HVGs, with an alpha threshold of 0.05.[44]

Gene distribution classes

For the three progenitor clusters from our NPC dataset, HVGs were classified into two categories: bimodal and unimodal genes. The multimode function from the multimode (1.5) R package was used to calculate the modes. To assess the differential proportion of genes in each class between genotypes, we employed the R implementation of the Pearson's χ^2 test with the chisq.test function. We performed the test for each of three progenitor clusters and then corrected for multiple comparison testing with the Benjamini-Hochberg method. An alpha threshold of 0.05 was used to evaluate significant differences in proportions between genotypes.

Histone modifications and TF enrichment analysis

The highest variable cluster within each dataset was selected for further analysis of HVGs and LVGs. We implemented the same gene selection criteria from the constraint analysis. The top 150 HVGs and LVGs with mean-normalized expression greater than 0.7 were used to determine associations with histone modifications and TF motifs. A lowered mean expression cutoff of 0.25 was employed to further investigate histone modification enrichment. The DESeq2-normalized values were employed for the expression cutoff. We used the Enrichr database, specifically the Epigenomics_Roadmap_HM_ChIP-seq and the ENCODE TF chromatin immunoprecipitation sequencing (ChIP-seq) datasets. We interfaced with the database using the enrichr R package (3.2).[45–47] More specifically, each HVG and LVG gene set from each dataset was compared to gene sets, available through the above-mentioned datasets, that are associated with histone modifications and TF binding sites. For the histone modification analysis, datasets from the Epigenomics Roadmap that were derived from fetal brain, H1-derived NPCs, H9, iPS DF 19.11, iPS DF 6.9, and hippocampus were included for visualization. Further, only H3K27ac, H3K4me3, H3K27me3, H3K4me1, and H3K36me3 were included for visualization. For TF motif analysis, the motifs with a minimum adjusted p value for enrichment among the five HVG and LVG datasets less than 1e−10 were displayed. Matrices were made using pheatmap R package (1.0.12).[48]

Gene-gene correlation analysis

We analyzed correlations between gene expression among HVGs and LVGs to assess intrinsic and extrinsic variability.[12,49–51] This analysis was performed for our three uncommitted progenitors, the three progenitor clusters from Qiu et al.,[21] and the three most variable oligodendrocyte clusters from Palmer et al.[22] Analysis was performed on each cluster independently. HVGs and LVGs that were shared between T21 and euploid conditions within each cluster were used for correlation analysis. We calculated the Pearson correlations in gene expression, using the SCTransform-normalized counts, between each gene pair using the cor function from the stats base R package (3.6.2). We performed this correlation within the T21 and euploid samples independently. We then subtracted the absolute value of the euploid correlation matrix from the absolute value of the T21 correlation matrix, such that negative values indicated a loss of correlation strength in T21. The resulting matrix was then hierarchically clustered. The hclust and dist functions from the stats base R package were implemented for hierarchical clustering and distance formula, respectively. We used the average method for hclust. This matrix was then visualized with ggplot2 (3.5.0).[31]

Results

T21 drives increased gene expression variability in human NPCs

To study early neurodevelopmental changes driven by T21, we first analyzed NPCs derived from isogenic human iPSC lines. The XY iPSC lines DS1 (T21) and DS2U (euploid) were previously derived from mosaic fibroblasts,[52] and we differentiated them into NPCs using dual SMAD inhibition (Figures 1A, S1A, and S1B). We then pooled NPCs from three wells per genotype after 3 weeks of differentiation *in vitro* and performed scRNA-seq using the 10× Genomics platform. With average depths of 120,035 and 133,463 reads per cell for the euploid and T21 samples, respectively, we obtained 19,816 cells (T21: 11,034, euploid: 8,782) before imposing cutoffs on the percentage of mitochondrial genes, unique molecular identifier (UMI) counts, and numbers of unique expressed genes and removing doublets from the samples (Figure S1C). Of the 18,262 cells that passed quality control (QC; T21: 10,052, euploid: 8,210), we grouped NPCs into six clusters: progenitor 1, progenitor 2, cycling progenitor, neuronal progenitor, gliogenic progenitor, and unknown (Figures 1B and S1D).

To quantify cell type variability, we used an established method.[32] Here, 12 statistical pipelines were compared and tested against simulated and experimentally generated scRNA-seq datasets to determine the most accurate methods to quantify biological variability across conditions.[32] The authors found the combination of TP10K normalization, including all genes, and denSNE reduction to perform optimally, with the differential variability metric being the distance to the medoid (Figure S1E).[32] Applying this method, we observed a significant increase in expression variability in T21 compared with the isogenic euploid control for five of the six clusters, including progenitor 1 (p_{adj} = 5.35e-14), progenitor 2 (p_{adj} = 1.57e−37), cycling progenitor (p_{adj} = 2.69e−08), neuronal progenitor (p_{adj} = 1.13e−09), and unknown

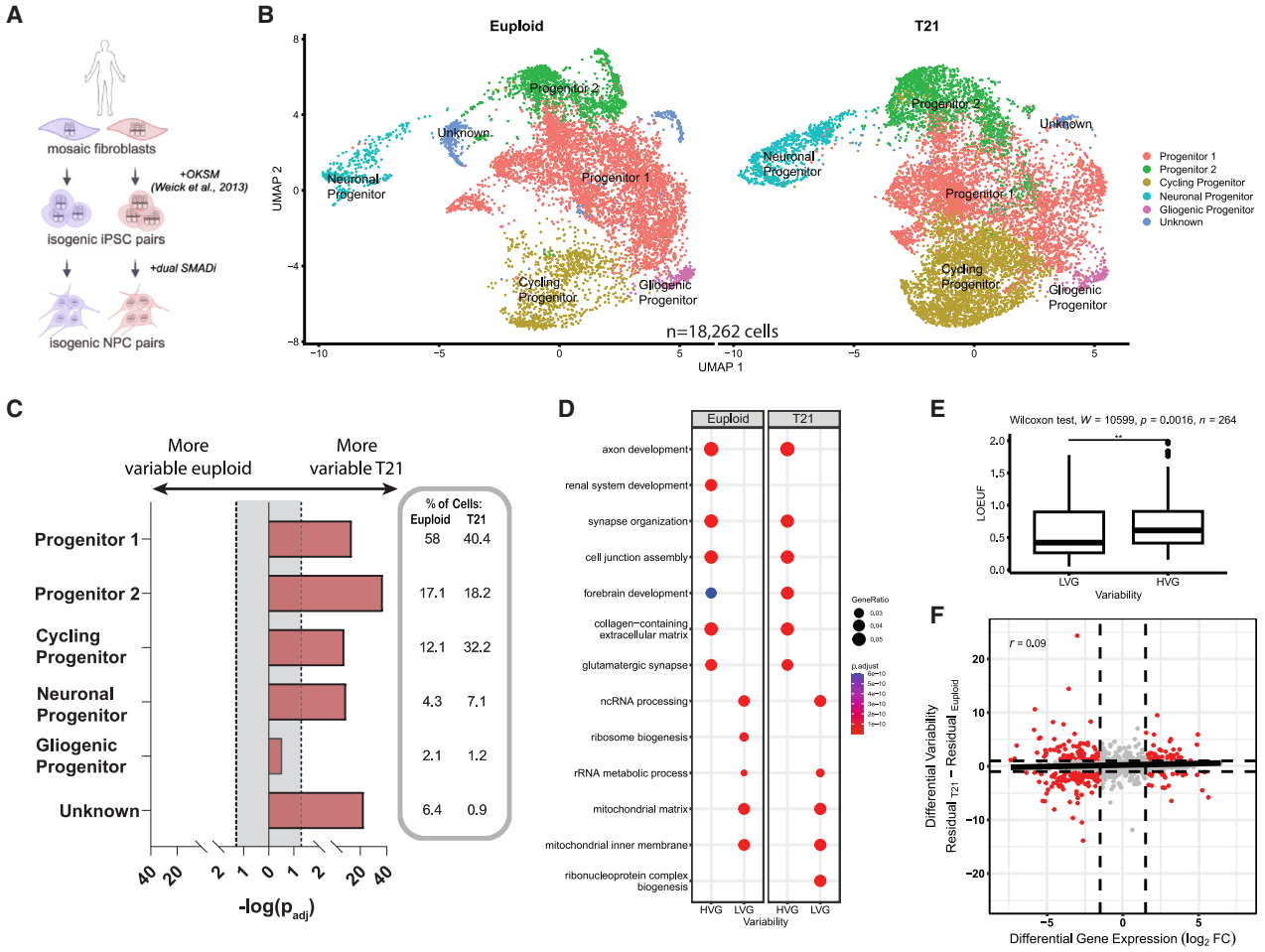

Figure 1. T21 drives increased gene expression variability in human NPCs

(A) Schematic of isogenic euploid and T21 NPCs used for scRNA-seq analysis.

(B) UMAP clustering of euploid and T21 NPCs (n = 18,262 cells) identifies six clusters: progenitor 1, progenitor 2, cycling progenitor, neuronal progenitor, gliogenic progenitor, and unknown.

(C) Cell type variability analysis between T21 and euploid NPCs for each of the six clusters. -log(p_{adj}) is shown on the x axis, with the gray shaded area indicating a lack of significance. More variable in T21 is indicated in red. The percentage of cells in each cluster for each genotype is shown on the right. Significance was determined by the two-sided Wilcoxon rank-sum test followed by Benjamini-Hochberg correction for multiple comparisons.

(D) GO analysis of HVGs and LVGs using the total list of genes present in three uncommitted progenitor clusters from euploid (left) and T21 (right) datasets (progenitor 1 [T21: 3,558 HVGs and 10,092 LVGs; euploid: 4,641 HVGs and 7,661 LVGs], cycling progenitor [T21: 2,519 HVGs and 12,713 LVGs; euploid: 2,432 HVGs and 13,928 LVGs], and progenitor 2 [T21: 3,366 HVGs and 9,256 LVGs; euploid: 2,252 HVGs and 13,496 LVGs] clusters). The color scale indicates p_{adj} values, and the circles are scaled to the gene ratio.

(E) Constraint analysis performed using gnomAD (v.4.1.0) to identify the LOEUF (loss-of-function observed/expected upper bound fraction) for the top 150 LVGs and HVGs from progenitor 2 cluster with a 0.7 mean-normalized expression cutoff (p = 0.0016). Of 300 genes in total, 264 had constraint data (HVG n = 121 and LVG n = 143). Significance was determined using the two-sided Wilcoxon test.

(F) Correlation between differential gene expression ($\log_2$FC) and differential variability (residual T21 − residual euploid) for the progenitor 2 cluster. Significant genes are shown in red. The Pearson correlation was 0.09.

All statistical significance was determined using an alpha threshold of 0.05. The schematic was created in BioRender.

(p_{adj} = 3.97e−23); over 97% of cells from each genotype belonged to clusters with increased variability in T21 (Figure 1C; Table S1). No cluster was more variable in the euploid condition (Figure 1C; Table S1). The distribution of the distance to medoid metric for the three uncommitted progenitor clusters (progenitor 1, cycling progenitor, and progenitor 2) also demonstrated that the increase in variability in T21 was not driven by outlier cells, as there were no isolated peaks with extreme distances (Figure S1F).

Next, we analyzed gene-level variability, controlling for expression levels.[38] Briefly, this method fits a GLM for the CV^2 and mean-normalized expression (Figure S2A). The ratio between the observed CV^2 and the expected CV^2 calculated using the GLM, the residual, provides a measure of the biological variability, which is not correlated with mean-normalized expression (Figure S2B). HVGs were defined as genes with a residual value greater than 1, as the observed CV^2 was greater than expected. LVGs were defined as genes with a residual value less

than 1, with the observed CV^2 less than expected. The residual sampling distribution was approximately a $\chi 2$ distribution; statistical significance was evaluated by performing a two-sided test of a $\chi 2$ distribution with the degrees of freedom being the number of cells minus 1.[38,39] Of note, multiple gene-level comparisons of variability from scRNA-seq versus single-molecule fluorescence *in situ* hybridization (FISH) report high concordance,[53,54] supporting scRNA-seq as a reliable data form from which to quantify variable genes.

As expected, HVGs showed broader gene density distributions at low (<0.25), medium ($1 > x > 0.25$), and high (>1) normalized mean expression categories compared with LVGs (Figure S2C). We focused on HVGs and LVGs from the three uncommitted progenitor clusters for further analysis. Using the combined list of genes from these clusters, GO analysis identified neural cell type and developmental terms enriched among the HVGs such as "axon development" (T21 p_{adj} = 2.3e−23 and euploid p_{adj} = 1.5e−28) and "forebrain development" (T21 p_{adj} = 4.0e−19 and euploid p_{adj} = 3.9e−10) (Figure 1D), while the LVGs were enriched for categories such as "non-coding RNA processing" (T21 p_{adj} = 2.9e−62 and euploid p_{adj} = 1.4e−59) and "mitochondrial matrix" (T21 p_{adj} = 9.0e−63 and euploid p_{adj} = 8.9e−64) not restricted to a specific cell type (Figure 1D). This is consistent with previous analyses of gene expression variability across normal human tissues or primary human cells, which found that more variable genes tended to function in development or associate with cell-type-specific functions, while less variable genes tended to be enriched for housekeeping functions.[39,55]

We next applied a constraint analysis using the genome aggregation database (gnomAD v.4.1.0). To reduce the impact of low expressed genes and focus on genes with greater variability deviations than expected, we selected the top 150 HVGs and LVGs from the progenitor 2 cluster by residual value and passing a mean-normalized expression cutoff of 0.70. Here, the top LVGs were associated with greater genetic constraint compared to HVGs, indicating reduced tolerance to variation (p = 0.0016; Figure 1E), consistent with our GO results (Figure 1D) and a previous study showing that LVGs are more likely to be loss-of-function intolerant compared with HVGs.[56]

We also performed differential gene expression analysis for the three uncommitted progenitor clusters to assess correlations between differential expression and differential variability. From progenitor 1, cycling progenitor, and progenitor 2 clusters, we identified 1,636 (935 upregulated and 701 downregulated), 1,144 (468 upregulated and 676 downregulated), and 1,548 (718 upregulated and 830 downregulated) differentially expressed genes (DEGs), respectively, using an alpha threshold of 0.05 and a $\log_2$ fold change ($\log_2$FC) cutoff of 1.5 (Table S2). Differential variability in gene expression and differential gene expression were poorly correlated in all three progenitor clusters (e.g., progenitor 2 cluster Pearson correlation, r = 0.09; Figures 1F and S2D), underscoring the independence of these two metrics.

To assess potential contributions of intrinsic versus extrinsic factors to the increased gene expression variability in T21, we generated gene-gene correlation matrices for HVGs and LVGs from each cluster. Variability driven by extrinsic factors spreads through coordinated gene regulatory networks, where these networks can be measured with gene-gene correlation matrices.[12,49] Thus, increased gene-gene correlation strength is consistent with the presence of gene co-expression networks and has previously been used as a measure of extrinsic (deterministic) variability, while decreased gene-gene correlation strength suggests a lack of gene regulatory networks and has thus been used as a measure of intrinsic (stochastic) variability.[12,49–51] As shown in Figures 2A and S2E, we observed decreased gene-gene correlation strength in T21 HVGs compared with isogenic euploid controls within the cycling progenitor cluster (mean change in correlation = −0.0272; n = 1,592 gene pairs) and progenitor 2 cluster (mean change in correlation = −0.0279; n = 1,442 gene pairs) while remaining unchanged for the progenitor 1 cluster (mean change in correlation = 0.0017; n = 2,731 gene pairs). For the cycling progenitor and progenitor 2 clusters, roughly 60% of gene-gene pairs showed a reduction in correlation strength in T21 (Figure 2A). For comparison, Desai et al. noted that approximately 80% of gene-gene pairs lost correlation strength following treatment with 5′-iodo-2′-deoxyuridine (IdU), a pyrimidine nucleotide identified as a top hit in a screen for enhancers of expression variability.[12] The reduced correlation strength observed within two of the three clusters in our data is consistent with intrinsic variability among the HVG networks in T21. For LVGs, gene-gene correlations remained largely unchanged between genotypes (Figure S2E), which may be related to their enrichment for genes with housekeeping functions.

Focusing on individual gene examples, we noted HVGs with a significant increase in variability in T21 compared to the isogenic euploid control with largely unimodal distribution patterns, such as the long non-coding RNA rhabdomyosarcoma 2-associated transcript (*RMST*) and the enzyme lactate dehydrogenase A (*LDHA*) (Figure 2B). Other genes showed a significant increase in variability in T21 but with a shift toward a more bimodal distribution pattern, such as the ephrin ligand ephrin A5 (*EFNA5*) and the cation channel transient receptor potential cation channel subfamily M member 3 (*TRPM3*) (Figure 2B). Focusing on expression differences, genes such as *TRPM3* had a robust $\log_2$FC (−2.30; $p < 1e{-}20$), but looking at the variability in expression revealed an on/off population structure (Figure 2B). Other genes, such as *EFNA5*, had a modest $\log_2$FC (0.135; p = 5.3e−10), but variability analysis showed two modes in T21, both of which differed from the isogenic euploid control (Figure 2B). Thus, focusing only on differential gene expression may exclude important information on

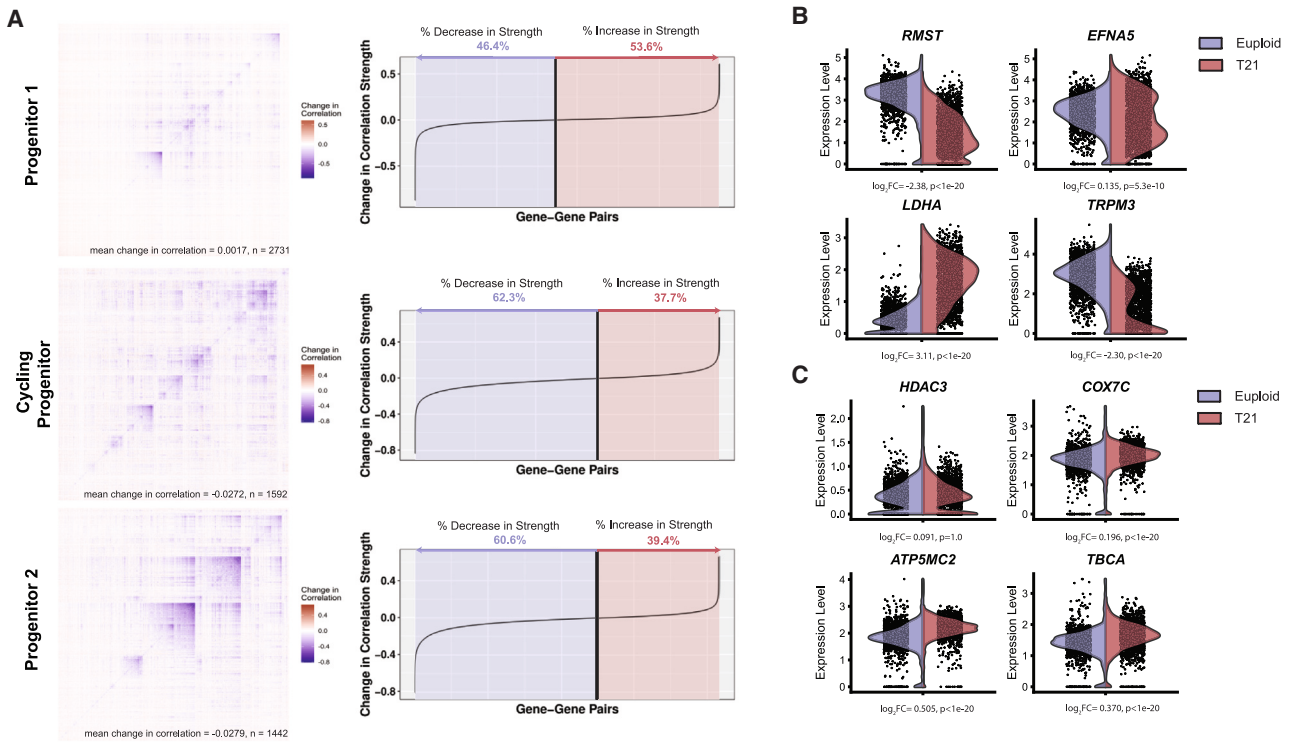

Figure 2. Decreased correlation strength in the T21 highly variable gene network points to intrinsic variability in human NPCs

(A) Matrices showing changes in gene-gene correlation strength for HVGs in the uncommitted progenitor clusters. Gene-gene correlations for each genotype were performed for HVGs in common between T21 and euploid conditions. Left, change in correlation strength between T21 and euploid conditions for progenitor 1 (top; mean change = 0.0017; $n = 2{,}731$ gene pairs), cycling progenitor (middle; mean change −0.0272; $n = 1{,}592$ gene pairs), and progenitor 2 (bottom; mean change = −0.0279; $n = 1{,}442$ gene pairs). Right, plotting the gene-gene pairs against the change in correlation shows the percentage of genes with increased or decreased correlation strength in T21 compared to euploid. Blue shading indicates loss in correlation strength in T21, with red shading illustrating increased correlation strength in T21.

(B) Violin plots showing expression levels of example HVGs from euploid (blue) and T21 (red) datasets including *RMST*, *LDHA*, *EFNA5*, and *TRPM3*. Log_2FC and p values of differential expression analysis are displayed below each violin plot.

(C) Violin plots showing expression levels of example LVGs from euploid (blue) and T21 (red) datasets including *HDAC3, ATP5MC2, COX7C*, and *TBCA*. Log_2FC and p values of differential expression analysis are displayed below each violin plot.

All statistical significance was determined using an alpha threshold of 0.05.

the cell-to-cell variability of gene expression in a given population. By contrast, individual LVGs, such as the chromatin remodeler histone deacetylase 3 (*HDAC3*), showed no change in expression or variability, while an enzyme of the mitochondrial electron transport chain, cytochrome *c* oxidase subunit 7C (*COX7C*), and the subunit of mitochondrial ATP synthase ATP synthase membrane subunit C locus 2 (*ATP5MC2*), showed no change in variability between genotypes but had a modest log_2FC (0.196, $p < 1e{-}20$ and 0.505, $p < 1e{-}20$, respectively) (Figure 2C). LVGs such as the tubulin chaperone factor tubulin folding cofactor A (*TBCA*) showed a modest increase in variability in T21 compared to the isogenic euploid control (Figure 2C).

As individual genes like *EFNA5* and *TRPM3* showed a shift toward bimodal distribution patterns in T21, previously associated with phenotypic variability,[57] we evaluated the proportions of bimodal versus unimodal HVGs from the three uncommitted progenitor clusters. Consistent with previous literature,[58] a majority of HVGs had a unimodal distribution pattern within all three clusters (Figure S2F). However, within the cycling progenitor cluster and progenitor 2 clusters, we found a significant increase in the proportion of genes with bimodal as opposed to unimodal distribution patterns ($p = 7.50e{-}4$), with no significant differences found in the progenitor 1 cluster ($p = 0.714$; Figure S2F).

Validation of T21-driven gene expression variability in an independent human NPC dataset

To confirm that the observed increased variability in T21 NPCs could be replicated in additional datasets, we first analyzed scRNA-seq data from Qiu et al.[21]; here, the authors generated scRNA-seq data using XY iPSCs from individuals with T21 and typically developing controls, which were then differentiated into NPCs.[21] After re-running the data analysis using Seurat v.5, we identified 10,678 cells (T21: 5,398, euploid: 5,280) that passed QC, grouped into seven clusters: progenitor 1, progenitor 2, progenitor 3, doublecortin (DCX)-expressing immature neurons, non-differentiated iPSCs 1 and 2, and oligodendrocyte progenitor cells (OPCs) (Figure 3A). Again, we observed

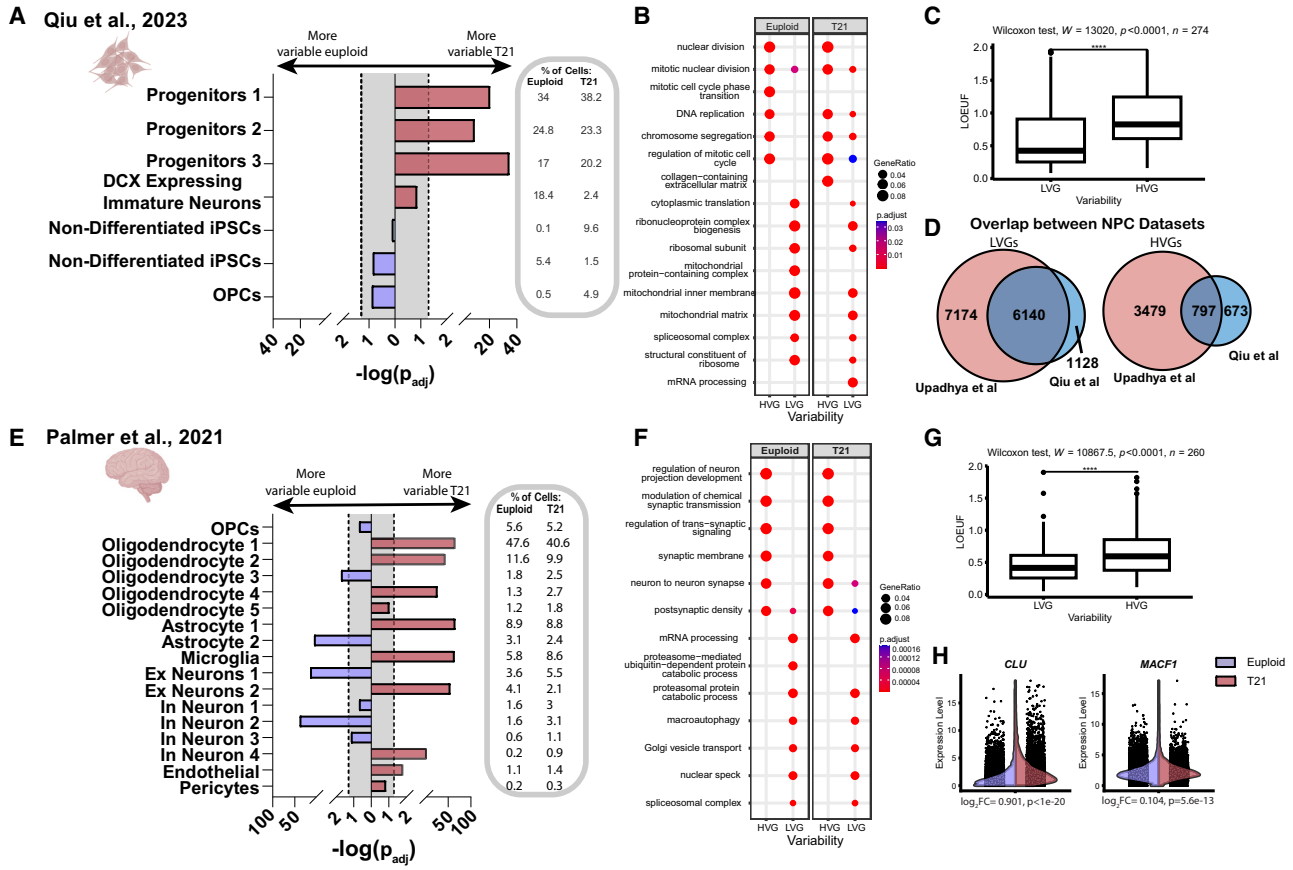

Figure 3. Validation of T21-driven gene expression variability in human NPCs and postmortem brain tissue

(A) Cell type variability analysis between T21 and euploid NPCs for each of seven clusters identified in Qiu et al.[21]. -log(p_{adj}) is shown on the x axis, with the gray shaded area indicating a lack of significance. More variable in T21 is indicated in red, and more variable in euploid is indicated in blue. The percentage of cells in each cluster for each genotype is shown on the right. Significance was determined by the two-sided Wilcoxon rank-sum test followed by Benjamini-Hochberg correction for multiple comparisons.

(B) GO analysis of HVGs and LVGs from euploid (left) and T21 (right) datasets from Qiu et al.[21] The color scale indicates p_{adj} values, and the circles are scaled to the gene ratio.

(C) Constraint analysis performed using gnomAD (v.4.1.0) to identify the LOEUF for the top 150 LVGs and HVGs from the Qiu et al.[21] dataset ($p < 0.0001$). Of the total 300 genes, 274 genes had constraint data (HVG $n = 140$, LVG $n = 134$). Significance was determined using the two-sided Wilcoxon test.

(D) Overlap analysis of LVGs (left) and HVGs (right) identified in progenitor clusters between our NPC dataset (Figure 1) and the Qiu et al.[21] NPC dataset.

(E) Cell type variability analysis between T21 and euploid human brain tissue for each of seventeen clusters identified in Palmer et al.[22] -log(p_{adj}) is shown on the x axis, with the gray shaded area indicating a lack of significance. More variable clusters in T21 are indicated in red, and more variable clusters in euploid are indicated in blue. The percentage of cells in each cluster for each genotype is shown on the right. Significance was determined by the two-sided Wilcoxon rank-sum test followed by Benjamini-Hochberg correction for multiple comparisons.

(F) GO analysis of HVGs and LVGs from euploid (left) and T21 (right) datasets from Palmer et al.[22] The color scale indicates p_{adj} values, and the circles are scaled to the gene ratio.

(G) Constraint analysis performed using gnomAD (v.4.1.0) to identify the LOEUF for the top 150 LVGs and HVGs from the Palmer et al.[22] dataset ($p < 0.0001$). Of the total 300 genes, 260 genes had constraint data (HVG $n = 113$, LVG $n = 147$). Significance was determined using the two-sided Wilcoxon test.

(H) Violin plots showing expression levels of an example HVG (*CLU*; left) and LVG (*MACF1*; right) from euploid and T21 astrocyte 1 cluster from Palmer et al.[22] Log_2FC and p values of differential expression analysis are displayed below each violin plot.

All statistical significance was determined using an alpha threshold of 0.05. The NPC and brain schematics were created in BioRender.

a significant increase in gene expression variability in T21 across all three uncommitted progenitor clusters, including progenitor 1 (p_{adj} = 5.53e−21), progenitor 2 (p_{adj} = 1.17e−09), and progenitor 3 (p_{adj} = 3.87e−35); over 75% of cells from each genotype belonged to clusters with increased variability in T21 (Figure 3A; Table S1), consistent with our findings above (Figure 1C). No cluster was significantly more variable in the euploid condition (Figure 3A; Table S1).

To assess gene-level variability, we first combined HVGs and LVGs from the three uncommitted progenitor clusters. GO analysis identified cell-cycle-related terms such as "nuclear division" (T21 p_{adj} = 8.1e−25, euploid p_{adj} = 3.0e−26) more enriched among the HVGs (Figure 3B), while terms

such as "ribonucleoprotein complex biogenesis" (T21 $p_{adj} = 10.0e{-}47$, euploid $p_{adj} = 6.2e{-}34$) or "mitochondrial matrix" (T21 $p_{adj} = 4.8e{-}47$, euploid $p_{adj} = 8.6e{-}32$) were associated with the LVGs (Figure 3B). Focusing on the progenitor 3 cluster and selecting the top 150 HVGs and LVGs by residual value and a mean-normalized expression cutoff of 0.70, the top LVGs were again associated with greater genetic constraint compared to HVGs ($p < 0.0001$; Figure 3C). Here, gene-gene correlation matrices for each cluster showed increased correlation strength in T21 for the HVGs (Figure S3A), suggesting that extrinsic factors may be influencing the HVG network in this dataset. For the LVGs, gene-gene correlations again remained largely unchanged between genotypes (Figure S3B). To query gene-level overlap between two independent NPC datasets, we compared HVGs and LVGs from the three uncommitted progenitor clusters from Qiu et al.[21] (Figure 3A) with the three uncommitted progenitor clusters from our data (Figures 1 and 2). A majority of LVGs overlapped between NPC datasets, while HVGs showed only partial overlap (Figure 3D), indicating that the identities of individual HVGs are more likely to vary between datasets.

Overall, analyses using different parental iPSC lines and *in vitro* differentiation paradigms from independently generated datasets support a significant increase in gene expression variability driven by T21 in human NPCs compared with euploid controls.

T21 drives increased gene expression variability in human brain tissue

To assess whether findings from human NPCs *in vitro* would extend to neural cell types in the human brain, we performed differential variability analysis using published snRNA-seq data generated from postmortem tissue.[22] These analyses included tissue from the prefrontal cortex (Brodmann areas 8/9) of nine individuals with T21 and 14 age-, sex-, and RIN (RNA integrity number)-matched unaffected control individuals.[22] After reanalyzing the data, we identified 147,383 cells (T21: 50,433, euploid: 96,950) grouped into 17 clusters, most of which were glial cell types. We observed a significant increase in gene expression variability in T21 compared to euploid control in 8 clusters; over 75% of cells from each genotype belonged to clusters with increased variability in T21 (Figure 3E; Table S1). Notably, the largest clusters were made up of oligodendrocytes, including oligodendrocytes 1 and 2, both of which showed significantly more variability in T21 compared to euploid controls ($p_{adj} < 1.66e{-}64$ and $p_{adj} = 4.47e{-}44$, respectively) (Figure 3E; Table S1). The next largest clusters were astrocyte 1 and microglia, which were again significantly more variable in T21 compared to euploid controls ($p_{adj} < 1.66e{-}64$ and $p_{adj} = 1.67e{-}64$, respectively) (Figure 3E; Table S1). Four clusters were significantly more variable in euploid control compared with T21, but these clusters included a minority of cells from each genotype; for example, inhibitory neuron 2, which included 1.6%–3.1% of cells from each genotype, was significantly more variable in euploid control compared with T21 ($p_{adj} = 1.38e{-}39$) (Figure 3E; Table S1). Overall, these results support our findings from human cellular models, with a majority of cells belonging to more variable clusters in T21 compared with euploid controls. As many cells included in the postmortem brain dataset were identified as oligodendrocytes, astrocytes, or microglia, the results here are most applicable to glial cell types.

Focusing on the three oligodendrocyte clusters that were more variable in T21 (oligodendrocyte 1, oligodendrocyte 2, and oligodendrocyte 4), GO analysis of all HVGs and LVGs identified neural cell-type-specific terms generally more enriched among the HVGs including "modulation of chemical synaptic transmission" (T21 $p_{adj} = 2.3e{-}13$ and euploid $p_{adj} = 4.3e{-}11$; Figure 3F) and terms such as "mRNA processing" (T21 $p_{adj} = 3.6e{-}50$ and euploid $p_{adj} = 7.7e{-}45$) not restricted to a specific cell type more enriched among the LVGs (Figure 3F). Using the top 150 HVGs and LVGs by residual value and a mean-normalized expression cutoff of 0.70, top LVGs from the oligodendrocyte 1 cluster were again associated with greater genetic constraint compared to HVGs ($p < 0.0001$; Figure 3G). Gene-gene correlations remained largely unchanged between genotypes (Figures S3C and S3D). Focusing on individual gene examples, in this case from astrocytes, HVGs such as the extracellular chaperone clusterin (*CLU*) showed increased variability in T21 compared to euploid controls; by contrast, LVGs such as the cytoskeletal gene microtubule actin crosslinking factor 1 (*MACF1*) showed no difference in variability between genotypes (Figure 3H).

Of note, buffering mechanisms such as nuclear transcript retention have previously been reported to reduce expression variability in the cytoplasm.[58,59] However, we found that both snRNA-seq and scRNA-seq datasets showed increased variability in transcript abundance in T21. Additionally, results from human cellular models were largely recapitulated in human brain tissue, supporting increased variability in both uncommitted NPCs and differentiated neural cell types.

Autism-associated CHD8 haploinsufficiency drives increased gene expression variability in human brain organoids

We next assessed whether syndromic neurodevelopmental conditions driven by mutations in epigenetic regulators could also show increased expression variability, reasoning that they could disrupt transcriptional processes or potentially impact gene dosage on a scale similar to that of an aneuploidy (i.e., hundreds of putative gene targets). Specifically, we analyzed published scRNA-seq datasets generated from human iPSC-derived organoid models engineered with mutations in high-confidence autism risk genes; gene mutations included lysine methyltransferase 5B (*KMT5B*; previous gene symbol *SUV420H1*) and the

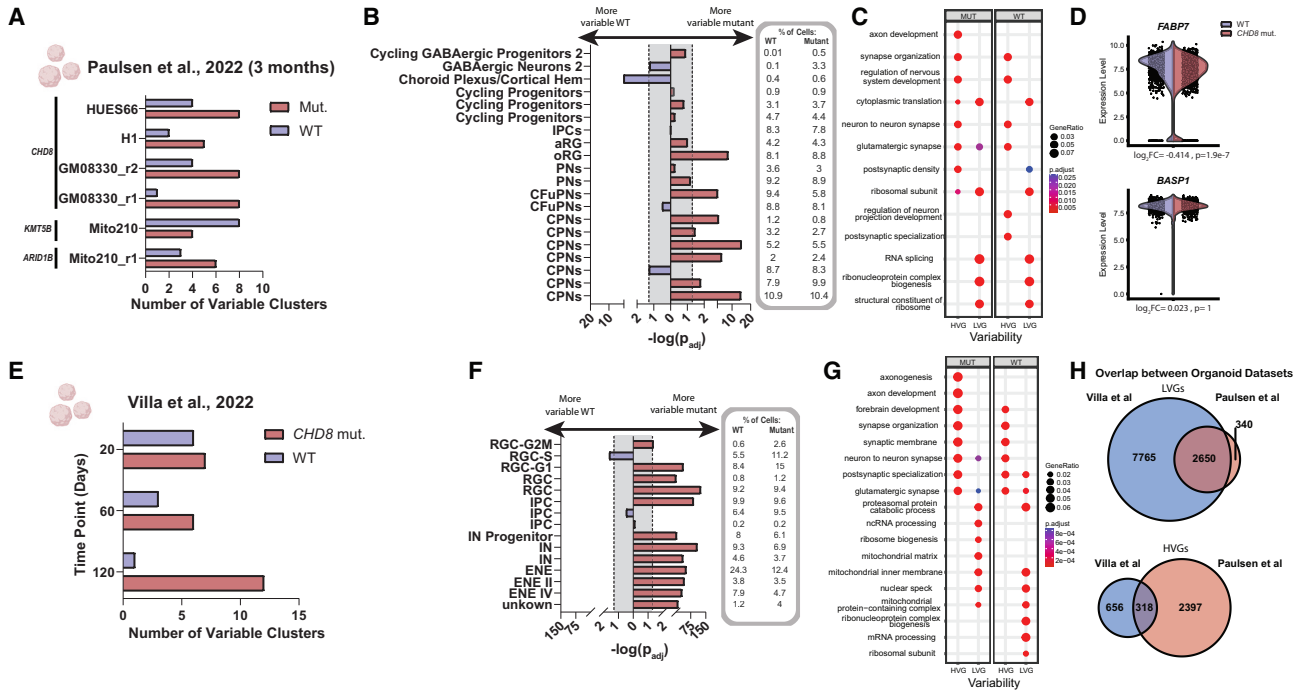

Figure 4. Autism-associated *CHD8* haploinsufficiency drives increased gene expression variability in human brain organoids

(A) Bar graph showing the number of variable clusters from 3-month organoids generated in independent genetic backgrounds (HUES66, H1, GM08330, and Mito210) and with different genotypes (*CHD8*, *KMT5B*, and *ARID1B*) from Paulsen et al.[23]

(B) Cell type variability analysis from an example *CHD8* mutant organoid (CHD8_GM_3m_r1) from Paulsen et al.[23] for each of 20 clusters. -log(p_{adj}) is shown on the x axis, with the gray shaded area indicating a lack of significance. More variable clusters in the *CHD8* mutant condition are indicated in red, and more variable clusters in the isogenic WT control are indicated in blue. The percentage of cells in each cluster for each genotype is shown on the right. Significance was determined by the two-sided Wilcoxon rank-sum test followed by Benjamini-Hochberg correction for multiple comparisons.

(C) GO analysis of *CHD8* mutant (left) and WT control (right) from an example *CHD8* mutant organoid (CHD8_GM_3m_r1) from Paulsen et al.[23] The color scale indicates p_{adj} values, and the circles are scaled to the gene ratio.

(D) Violin plots showing expression levels of an example HVG (*FABP7*; top) and LVG (*BASP1*; bottom) from *CHD8* mutant and control CPNs from *CHD8* mutant organoid (CHD8_GM_3m_r1) from Paulsen et al.[23] Log_2FC and *p* values of differential expression analysis are displayed below each violin plot.

(E) Bar graph showing the number of variable clusters from *CHD8* mutant organoids at 20, 60, and 120 days from Villa et al.[24]

(F) Cell type variability analysis of the 120-day time point *CHD8* mutant organoid from Villa et al.[24] for each of 15 clusters. -log(p_{adj}) is shown on the x axis, with the gray shaded area indicating a lack of significance. More variable clusters in the *CHD8* mutant condition are indicated in red, and more variable clusters in WT control are indicated in blue. The percentage of cells in each cluster for each genotype is shown on the right. Significance was determined by the two-sided Wilcoxon rank-sum test followed by Benjamini-Hochberg correction for multiple comparisons.

(G) GO analysis of *CHD8* mutant (left) and WT control (right) from the 120-day time point *CHD8* mutant organoid from Villa et al.[24] The color scale indicates p_{adj} values, and the circles are scaled to the gene ratio.

(H) Overlap analysis between LVGs (top) and HVGs (bottom) from Paulsen et al.[23] CPNs from CHD8_GM_3m_r1 and Villa et al.[24] ENEs from 120-day organoids.

All statistical significance was determined using an alpha threshold of 0.05. The organoid schematics were created in BioRender.

chromatin remodeling factors *CHD8* and AT-rich interaction domain 1B (*ARID1B*).[23,24]

Paulsen et al.[23] generated organoids from multiple independent genetic backgrounds engineered with mutations in *KMT5B*, *CHD8*, and *ARID1B*.[23] At 3 months, *CHD8* loss led to an increase in the number of variable organoid clusters compared with the respective isogenic controls for each of three different genetic backgrounds (HUES66, H1, and GM08330; Figures 4A and S4A–S4C). Focusing on the *CHD8* mutation in the GM08330 genetic background as an individual organoid example, we identified 34,951 cells (mutant [Mut]: 20,334, WT: 14,617) across 20 clusters (Figure 4B). We observed a significant increase in gene expression variability with loss of *CHD8* compared to isogenic controls in eight clusters; roughly 50% of cells in each dataset belonged to clusters with increased variability in the *CHD8* Mut condition (Figure 4B; Table S1). By contrast, only one cluster was more variable in the isogenic control condition, which included <1% of cells from each genotype (Figure 4B; Table S1). Here, most cell types were identified as neuronal, with more variable clusters in the *CHD8* Mut condition including CPNs, outer radial glia (oRGs), and corticofugal projection neurons (CFuPNs) (Figure 4B; Table S1). This finding was in contrast to *ARID1B* and *KMT5B* mutations, which did not show convincing trends toward increased expression variability in these datasets (Figures 4A, S4D, and S4E; Table S1).

To assess gene-level variability, we selected the top three most variable CPN clusters within the *CHD8* Mut condition, again using all unique HVGs and LVGs between the three clusters for GO analysis. HVGs were more likely to be associated with neural cell-type-specific terms such as "synapse organization" (Mut p_{adj} = 1.7e−10, WT p_{adj} = 6.7e−11), while LVGs were more likely to be associated with terms such as "RNA splicing" (Mut p_{adj} = 1.2e−33, WT p_{adj} = 1.2e−30; Figure 4C). Focusing on individual gene examples from CPNs, HVGs such as the autism risk gene fatty acid binding protein 7 (*FABP7*) showed increased variability in the *CHD8* Mut condition compared to the isogenic control, in contrast to LVGs such as the signaling gene brain abundant membrane attached signal protein 1 (*BASP1*), which showed no difference in variability between genotypes (Figure 4D). Here, applying constraint analysis on the most variable CPN cluster did not identify a significant relationship with LVGs, only a non-significant trend ($p = 0.120$; Figure S4F).

To confirm the observed increased gene expression variability in the *CHD8* Mut condition, we leveraged an independent human iPSC-derived organoid scRNA-seq dataset from Villa et al.,[24] driven by distinct *CHD8* mutations and using iPSC lines independent of those used in Paulsen et al.[23] Here, the number of variable clusters per organoid increased over time, with the 120-day time point showing the largest number of variable clusters with loss of *CHD8* compared to isogenic controls (Figures 4E, S4G, and S4H). Focusing on the 120-day time point, we identified 20,940 cells (Mut: 14,261, WT: 6,679) across 15 clusters (Figure 4F; Table S1). A significant increase in gene expression variability was evident across 12 clusters; over 79% of cells from each genotype belonged to clusters with increased variability in the *CHD8* Mut condition, including both proliferating cell types (e.g., radial glial cells [RGCs]) and differentiated cell types (e.g., interneurons [INs] and excitatory neurons early [ENEs]) (Figure 4F; Table S1). To probe gene-level variability, we focused on the three ENE clusters ENE, ENEII, and ENEIV. Again, gene-level analyses showed HVGs more enriched for terms such as "synapse organization" (Mut p_{adj} = 1.3e−21, WT p_{adj} = 9.8e−20), with LVGs more likely to be associated with non-cell-type-specific terms such as "mitochondrial inner membrane" (Mut p_{adj} = 1.4e−42, WT p_{adj} = 8.5e−34; Figure 4G). In contrast to other datasets, constraint analysis identified top LVGs as less constrained compared with HVGs within the ENE cluster ($p < 0.0001$; Figure S4I). To query gene-level overlap between independent *CHD8* Mut organoid datasets, we focused on neuronal cells, comparing HVGs and LVGs identified from the three most variable CPN clusters in Paulsen et al.[23] (Figure 4B), with HVGs and LVGs identified from the three ENE clusters in Villa et al.[24] (Figure 4F). Similar to our results comparing T21 NPC datasets (Figure 3D), a majority of LVGs overlapped between neuronal cell types in the organoid datasets, with HVGs showing only partial overlap (Figure 4H).

Collectively, these results indicate that loss of the chromatin remodeling factor *CHD8* can also drive increased variability in gene expression in human neural cell types.

Molecular basis of gene expression variability

To identify potential underlying mechanisms, we analyzed the five independent human scRNA-seq or snRNA-seq datasets discussed above, including our scRNA-seq data from T21 and euploid control NPCs, combined with two published T21 datasets[21,22] and two published *CHD8* Mut datasets.[23,24] This strategy gave us the opportunity to look at variable genes across different conditions and datasets to extract common principles.

We first assessed the association of HVGs and LVGs with the genome-wide distributions of active and repressive histone marks using NIH Roadmap Epigenomics data.[47] For each dataset, we took the top 150 significant HVGs and LVGs from the most variable cluster in disease that met a threshold of mean-normalized expression greater than 0.70 so that all datasets had equal numbers of HVGs and LVGs for enrichment analyses. We found that LVGs were enriched for active marks such as H3K27ac and H3K4me3, while HVGs showed no specific enrichment pattern (Figure 5A). Lowering the mean-normalized expression threshold to 0.25 preserved the association of LVGs with H3K27ac and H3K4me3 and also revealed a modest correlation of HVGs with the repressive mark H3K27me3 across four of the five independent datasets (Figure 5A). H3K27me3 plays important roles in silencing tissue-specific genes during development, and the correlation between H3K27me3 and HVGs at a low expression threshold is consistent with a previous study showing an association between PRC2/H3K27me3 and genes with higher variability in mouse embryonic stem cells.[53]

We also examined TF binding motifs enriched in each set of HVGs and LVGs. As with the histone analysis, we used the top 150 significant HVGs and LVGs from each dataset with mean-normalized expression greater than 0.7 to evaluate enrichment with ENCODE TF ChIP-seq data.[46] Focusing on the top 58 most enriched motifs (minimum $p_{adj} < 1e{-}10$), those with the strongest enrichment across multiple HVG datasets were lysine acetyltransferase 2A (*KAT2A*), a histone acetyltransferase, and negative elongation factor complex member E (*NELFE*), part of a complex mediating RNA polymerase II (RNA Pol II) pausing at proximal promoters (Figures 5B and 5C). However, both *KAT2A* and *NELFE* motifs were enriched to a greater extent across LVGs from multiple datasets (Figures 5B and 5C), indicating their lack of specificity for HVGs. Motifs for several transcriptional regulators, such as forkhead box M1 (*FOXM1*), were uniquely enriched in HVGs but only for a single dataset (Figures 5B and 5C). Indeed, we were unable to identify any motif specifically and consistently associated with HVGs, paralleling the lack of pathway specificity identified for the HVGs by GO analysis (Figures 1D, 3B, 3F, 4C, and 4G). By contrast, multiple motifs were specifically and consistently enriched across LVGs from multiple datasets, such as YY1 TF (*YY1*) (Figures 5B and 5C), suggesting

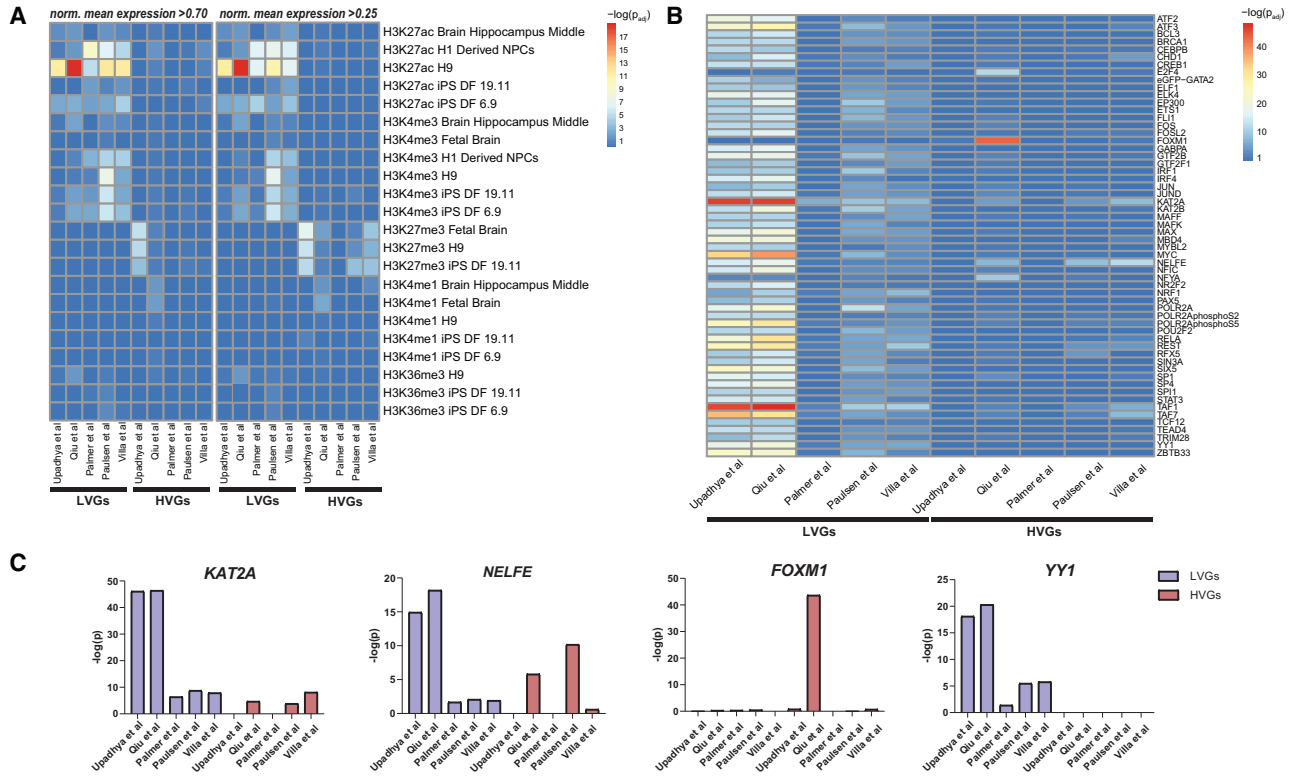

Figure 5. Molecular basis of gene expression variability

(A) Heatmap of enriched histone post-translational modifications (PTMs) for HVGs and LVGs from the most variable cluster from each dataset (Upadhya et al. [this study], Qiu et al.,[21] Palmer et al.,[22] Paulsen et al.[23] *CHD8* mutant organoid [CHD8_GM_3m_r1], and Villa et al.[24] 120-day *CHD8* mutant organoid). The left heatmap was made with the top 150 genes based on gene residuals that met the normalized mean expression cutoff of 0.70, and the right heatmap was made with the top 150 genes based on gene residuals that met the normalized mean expression cutoff of 0.25. Data from the Epigenomics Roadmap ChIP-seq data through Enrichr were used to evaluate enrichment. The color scale indicates the -log(p_{adj}) level of gene set enrichment.

(B) Heatmap of enriched transcription factor motifs with HVGs and LVGs from the most variable cluster from each dataset (Upadhya et al. [this study], Qiu et al.,[21] Palmer et al.,[22] Paulsen et al.[23] *CHD8* mutant organoid [CHD8_GM_3m_r1], and Villa et al.[24] 120-day *CHD8* mutant organoid). Data from the ENCODE TF ChIP-seq dataset through Enrichr were used to evaluate enrichment of the top 150 HVGs and LVGs that met the mean-normalized mean expression cutoff of 0.70. The color scale indicates the -log(p_{adj}) level of gene set enrichment.

(C) Bar graphs showing examples of individual transcriptional regulators significantly enriched in LVGs and/or HVGs. Motifs with a minimum adjusted *p* value for enrichment <1e−10 are displayed. LVGs are shown in blue and HVGs in red, with -log(p_{adj}) on the y axis. All statistical significance was determined using an alpha threshold of 0.05.

that LVGs are more likely than HVGs to share overlapping regulatory elements.

Collectively, these data highlight the association of LVGs with transcriptional activity across multiple datasets but do not identify a specific signature associated with HVGs beyond modest enrichment of H3K27me3 at low expression thresholds. The features of variable genes identified here match the features of variable genes identified in other systems, including the association of LVGs with active transcription, housekeeping genes, and reduced tolerance to loss-of-function mutations and the association of HVGs with H3K27me3 and cell-type-specific genes,[39,53,55,56] further confirming the accuracy of our analyses.

Discussion

Here, we identify increased gene expression variability driven by the autosomal aneuploidy T21 as well as loss of the high-confidence autism-associated gene *CHD8* in human brain-relevant cell and tissue types. Cell-to-cell variability in molecular expression during development, aging, and disease is well documented, and our results extend these findings to human neurodevelopmental conditions, underscoring the importance of understanding differential gene expression variability in addition to differential gene expression.

Mechanistically, molecular variability could originate transcriptionally and propagate through post-transcriptional processes or, alternatively, be generated post-transcriptionally. In the case of T21, we speculate that the fidelity of transcription is negatively impacted by dramatic changes in gene dosage. This would be consistent with our finding of increased variability in both scRNA-seq as well as snRNA-seq datasets. Post-transcriptional sources of variability could include degradation or unequal partitioning of molecules during cell division.[7,8] Emerging technologies, such as pulse-chase labeling combined with

scRNA-seq, have been used to model contributions of transcription versus mRNA decay to variability[60] and could be used to further address this question. The shift toward bimodal gene expression in T21 has previously been associated with phenotypic diversity; several potential mechanisms, including feedback loops and transcriptional bursting (stochastic switching between ON and OFF states), have been associated with bimodal gene expression[57] and could thus be contributing to this pattern in T21. It is also possible that cellular stress in disease could lead to bet hedging to increase fitness at a population level, although bet hedging has been more extensively studied in prokaryotes than eukaryotes.[4,61,62] Finally, increased promoter accessibility has been correlated with reduced gene expression variability at select loci in HeLa cells.[63] Multiomics analyses (snRNA-seq and snATAC-seq) could be used to determine whether increased variability correlates with a more closed chromatin structure, implicating an epigenetic mechanism.

In addition to identifying underlying mechanisms, an important next step will be determining how gene expression variability translates to protein variability and the impacts on specific cellular phenotypes. Several studies report that gene-level variability can be detected at the protein level through candidate analyses.[12,64,65] For example, Hansen et al. report that "transcriptional noise" is amplified during the downstream processes of mRNA nuclear export, translation, and mRNA degradation, leading to higher variability in transcript abundance in the cytoplasm than the nucleus and ultimately propagating to generate protein-level variability.[64] However, factors such as protein half-life[12] and quality control of orphan proteins may also influence protein-level variability, underscoring the importance of querying diverse candidates. Cellular phenotypes could also be tested using *in vitro* models to further understand the impact of expression variability on phenotypic outcome. For example, Hwang et al. report variability in fibroblast nuclear morphology due to T21, consistent with previous findings in yeast,[66] and it would be interesting to assess this phenotype in neural cells. Given our GO analyses of the HVG network, we may expect to see variability in synaptic development in T21; previous studies have identified significant changes in synaptic development in T21,[67] but variability in the penetrance or expressivity of this phenotype has not been assessed. Finally, several studies have used screening approaches to look for modulators of expression variability on other cellular systems[53,68]; the ability to dynamically modulate variability in neural cells would facilitate further investigation of functional relevance.

Our results challenge assumptions inherent in many disease modeling studies: that phenotypes are genetically encoded (and are therefore stably preserved in the model) and that cross-study differences are due to technical factors (and are therefore controllable). At a minimum, studies may need increased sample numbers, including donor individuals and replicates, to account for increased biological variability. Moreover, focusing on the statistical mean and excluding the spread of the data may obfuscate important information.[69] In the case of T21, the precise anatomical, cellular, and molecular changes driving specific phenotypes remain actively debated in the field.[67] Our findings of increased expression variability in T21 are consistent with the profound interindividual variation in T21 phenotypes and low concordance observed across experimental studies.[2,3,67] While phenotypic variability has been well documented in T21, given the condition's high prevalence, this phenomenon remains less well defined for rare conditions like *CHD8* haploinsufficiency. The generation of additional powered datasets at the single-cell level will be required to ascertain which genetic or chromosomal alterations lead to increased variability.

Of note, individual datasets showed differences in their variability profiles. In contrast to our data, the increased gene-gene correlation strength in T21 observed in NPCs from Qiu et al.[21] highlights that extrinsic conditions can also influence variability. However, the increased variability observed in T21 from multiple cell and tissue sources and independent studies makes a consistent difference in an extrinsic regulatory factor unlikely. While gene-gene correlation strength is used to estimate intrinsic versus extrinsic contributions to variability,[12,49–51] additional strategies such as dual-reporter methods to query candidate genes[70] or emerging strategies to measure allele-specific expression from scRNA-seq data[71] could potentially be used to strengthen our finding of intrinsic variability in T21. We speculate that differences in extrinsic versus intrinsic variability coupled with independent genetic backgrounds together may influence the identities of the specific variable genes, which diverged across datasets. Moreover, if disease drives an increase in stochastic variability, we may expect less overlap between HVGs, which do not appear to coalesce into a single category beyond a brain cell type association, while the genes intolerant to variability (LVGs) may be more likely to be consistent across datasets. Also of note was the lack of consistent increased expression variability from organoids with *ARID1B* and *KMT5B* mutations in contrast to organoids with *CHD8* mutations. These three risk genes were shown to have different molecular mechanisms.[23] It is possible that variability is influenced by the scale at which specific mutations alter gene dosage (e.g., the total number of gene targets disrupted) or the specific transcriptional or post-transcriptional processes that are disrupted. Additionally, several of the datasets analyzed were primarily made up of one major cell classification (e.g., NPCs in our data and Qiu et al.[21] and glial cell types in Palmer et al.[22]). Thus, it is not possible to ascertain whether different neural cell types are more or less susceptible to gene expression variability in T21, which will be an interesting question to address in future studies.

Several additional open questions remain. First, our analyses focus on human neurodevelopmental conditions and brain cell types, but whether variability may be fundamentally different across species, organ systems, or developmental stages remains to be determined. Second, the

extent to which variable cell states are heritable remains unknown. Previous work in budding yeast found that variability in cell cycle kinetics was not consistent from division to division, suggesting a lack of genetic or epigenetic heritability.[4] In the case of TRAIL-mediated apoptosis in human cancer cell lines, variability was shown to be transiently heritable based on protein states.[15] Further work will be required to determine what non-genetic information may be transmitted and for how long. Third, the quantification of cell-to-cell variability at epigenomic, metabolomic, or proteomic levels, in addition to variability in the spatial organization of molecules, is also of high relevance but less frequently captured at scale compared with transcriptomic measurements. It will be particularly interesting in future studies to understand variability in co-transcriptional processes like alternative splicing or post-transcriptional processes like trafficking/localization and how this may impact function. The rapid expansion in single-cell omics technologies will provide tremendous opportunity to understand variability and explore potential underlying mechanisms in different data forms across normal and disease conditions. Finally, it remains to be determined whether increased variability during embryogenesis *in vivo* could ultimately contribute to diverse developmental trajectories.

Data and code availability

scRNA-seq data have been deposited at GEO: GSE279894. Code is available at https://github.com/suraj-upad/Transcriptional_variance_T21.

Acknowledgments

We are indebted to members of the Barrett lab as well as to Olli Pietiläinen for their insightful comments and suggestions on this project. We also thank the Harvard University Bauer Sequencing Core for assistance with scRNA-seq and the Chun lab data access committee for assistance with accessing human brain sequencing datasets. This work was supported by NIH grants R01HD101534 and R01HD111876 to L.E.B.

Author contributions

L.E.B. and S.U. conceived the study and wrote the manuscript; S.U., J.A.K., and A.N. generated cells for the study; S.U. and J.A.K. performed scRNA-seq and analysis; S.U. performed all other analyses with guidance from K.M.H.; and L.E.B. supervised the study and secured funding. All authors discussed the results and edited the manuscript.

Declaration of interests

The authors declare no competing interests.

Supplemental information

Supplemental information can be found online at https://doi.org/10.1016/j.ajhg.2025.02.011.

Web resources

ArrayExpress, https://www.ebi.ac.uk/biostudies/arrayexpress
European Genome-Phenome Archive, https://ega-archive.org
GEO, https://www.ncbi.nlm.nih.gov/geo/

Received: October 28, 2024
Accepted: February 10, 2025
Published: March 7, 2025

References

1. Roper, R.J., and Reeves, R.H. (2006). Understanding the basis for Down syndrome phenotypes. PLoS Genet. *2*, e50.
2. Antonarakis, S.E., Skotko, B.G., Rafii, M.S., Strydom, A., Pape, S.E., Bianchi, D.W., Sherman, S.L., and Reeves, R.H. (2020). Down syndrome. Nat. Rev. Dis. Primers *6*, 9–20.
3. Thomas, M.S.C., Ojinaga Alfageme, O., D'Souza, H., Patkee, P.A., Rutherford, M.A., Mok, K.Y., Hardy, J., Karmiloff-Smith, A.; and LonDownS Consortium (2020). A multi-level developmental approach to exploring individual differences in Down syndrome: genes, brain, behaviour, and environment. Res. Dev. Disabil. *104*, 103638.
4. Beach, R.R., Ricci-Tam, C., Brennan, C.M., Moomau, C.A., Hsu, P.-H., Hua, B., Silberman, R.E., Springer, M., and Amon, A. (2017). Aneuploidy Causes Non-genetic Individuality. Cell *169*, 229–242.e21.
5. Pavelka, N., Rancati, G., Zhu, J., Bradford, W.D., Saraf, A., Florens, L., Sanderson, B.W., Hattem, G.L., and Li, R. (2010). Aneuploidy confers quantitative proteome changes and phenotypic variation in budding yeast. Nature *468*, 321–325.
6. Kanata, E., Duffié, R., and Schulz, E.G. (2024). Establishment and maintenance of random monoallelic expression. Development *151*, dev201741. https://doi.org/10.1242/dev.201741.
7. Raj, A., and van Oudenaarden, A. (2008). Nature, nurture, or chance: stochastic gene expression and its consequences. Cell *135*, 216–226.
8. Loewer, A., and Lahav, G. (2011). We are all individuals: causes and consequences of non-genetic heterogeneity in mammalian cells. Curr. Opin. Genet. Dev. *21*, 753–758.
9. Snijder, B., and Pelkmans, L. (2011). Origins of regulated cell-to-cell variability. Nat. Rev. Mol. Cell Biol. *12*, 119–125.
10. Snijder, B., Sacher, R., Rämö, P., Damm, E.-M., Liberali, P., and Pelkmans, L. (2009). Population context determines cell-to-cell variability in endocytosis and virus infection. Nature *461*, 520–523.
11. Ohnishi, Y., Huber, W., Tsumura, A., Kang, M., Xenopoulos, P., Kurimoto, K., Oleś, A.K., Araúzo-Bravo, M.J., Saitou, M., Hadjantonakis, A.-K., and Hiiragi, T. (2014). Cell-to-cell expression variability followed by signal reinforcement progressively segregates early mouse lineages. Nat. Cell Biol. *16*, 27–37.
12. Desai, R.V., Chen, X., Martin, B., Chaturvedi, S., Hwang, D.W., Li, W., Yu, C., Ding, S., Thomson, M., Singer, R.H., et al. (2021). A DNA repair pathway can regulate transcriptional noise to promote cell fate transitions. Science *373*, eabc6506. https://doi.org/10.1126/science.abc6506.
13. Goolam, M., Scialdone, A., Graham, S.J.L., Macaulay, I.C., Jedrusik, A., Hupalowska, A., Voet, T., Marioni, J.C., and Zernicka-Goetz, M. (2016). Heterogeneity in Oct4 and Sox2 Targets Biases Cell Fate in 4-Cell Mouse Embryos. Cell *165*, 61–74.

14. Chang, H.H., Hemberg, M., Barahona, M., Ingber, D.E., and Huang, S. (2008). Transcriptome-wide noise controls lineage choice in mammalian progenitor cells. Nature *453*, 544–547.
15. Spencer, S.L., Gaudet, S., Albeck, J.G., Burke, J.M., and Sorger, P.K. (2009). Non-genetic origins of cell-to-cell variability in TRAIL-induced apoptosis. Nature *459*, 428–432.
16. Goyal, Y., Busch, G.T., Pillai, M., Li, J., Boe, R.H., Grody, E.I., Chelvanambi, M., Dardani, I.P., Emert, B., Bodkin, N., et al. (2023). Diverse clonal fates emerge upon drug treatment of homogeneous cancer cells. Nature *620*, 651–659.
17. Bahar, R., Hartmann, C.H., Rodriguez, K.A., Denny, A.D., Busuttil, R.A., Dollé, M.E.T., Calder, R.B., Chisholm, G.B., Pollock, B.H., Klein, C.A., and Vijg, J. (2006). Increased cell-to-cell variation in gene expression in ageing mouse heart. Nature *441*, 1011–1014.
18. Martinez-Jimenez, C.P., Eling, N., Chen, H.-C., Vallejos, C.A., Kolodziejczyk, A.A., Connor, F., Stojic, L., Rayner, T.F., Stubbington, M.J.T., Teichmann, S.A., et al. (2017). Aging increases cell-to-cell transcriptional variability upon immune stimulation. Science *355*, 1433–1436.
19. Debès, C., Papadakis, A., Grönke, S., Karalay, Ö., Tain, L.S., Mizi, A., Nakamura, S., Hahn, O., Weigelt, C., Josipovic, N., et al. (2023). Ageing-associated changes in transcriptional elongation influence longevity. Nature *616*, 814–821.
20. Zheng, G.X.Y., Terry, J.M., Belgrader, P., Ryvkin, P., Bent, Z.W., Wilson, R., Ziraldo, S.B., Wheeler, T.D., McDermott, G.P., Zhu, J., et al. (2017). Massively parallel digital transcriptional profiling of single cells. Nat. Commun. *8*, 14049.
21. Qiu, J.-J., Liu, Y.-N., Wei, H., Zeng, F., and Yan, J.-B. (2023). Single-cell RNA sequencing of neural stem cells derived from human trisomic iPSCs reveals the abnormalities during neural differentiation of Down syndrome. Front. Mol. Neurosci. *16*, 1137123.
22. Palmer, C.R., Liu, C.S., Romanow, W.J., Lee, M.-H., and Chun, J. (2021). Altered cell and RNA isoform diversity in aging Down syndrome brains. Proc. Natl. Acad. Sci. USA *118*, e2114326118. https://doi.org/10.1073/pnas.2114326118.
23. Paulsen, B., Velasco, S., Kedaigle, A.J., Pigoni, M., Quadrato, G., Deo, A.J., Adiconis, X., Uzquiano, A., Sartore, R., Yang, S.M., et al. (2022). Autism genes converge on asynchronous development of shared neuron classes. Nature *602*, 268–273.
24. Villa, C.E., Cheroni, C., Dotter, C.P., López-Tóbon, A., Oliveira, B., Sacco, R., Yahya, A.Ç., Morandell, J., Gabriele, M., Tavakoli, M.R., et al. (2022). CHD8 haploinsufficiency links autism to transient alterations in excitatory and inhibitory trajectories. Cell Rep. *39*, 110615.
25. Butler, A., Hoffman, P., Smibert, P., Papalexi, E., and Satija, R. (2018). Integrating single-cell transcriptomic data across different conditions, technologies, and species. Nat. Biotechnol. *36*, 411–420.
26. Hafemeister, C., and Satija, R. (2019). Normalization and variance stabilization of single-cell RNA-seq data using regularized negative binomial regression. Genome Biol. *20*, 296.
27. R Core Team (2022). R: A Language and Environment for Statistical Computing (Vienna, Austria: R Foundation for Statistical Computing). https://www.R-project.org.
28. McGinnis, C.S., Murrow, L.M., and Gartner, Z.J. (2019). DoubletFinder: Doublet detection in single-cell RNA sequencing data using artificial nearest neighbors. Cell Syst. *8*, 329–337.e4.
29. Korsunsky, I., Millard, N., Fan, J., Slowikowski, K., Zhang, F., Wei, K., Baglaenko, Y., Brenner, M., Loh, P.-R., and Raychaudhuri, S. (2019). Fast, sensitive and accurate integration of single-cell data with Harmony. Nat. Methods *16*, 1289–1296.
30. Wilcoxon, F. (1945). Individual comparisons by ranking methods. Biom. Bull. (Arch. Am. Art) *1*, 80.
31. Wickham, H. (2009). Ggplot2: Elegant Graphics for Data Analysis, 1st ed. (Springer).
32. Liu, J., Kreimer, A., and Li, W.V. (2023). Differential variability analysis of single-cell gene expression data. Brief. Bioinform. *24*, bbad294. https://doi.org/10.1093/bib/bbad294.
33. Narayan, A., Berger, B., and Cho, H. (2021). Assessing single-cell transcriptomic variability through density-preserving data visualization. Nat. Biotechnol. *39*, 765–774.
34. Pedregosa, F., Varoquaux, G., Gramfort, A., Michel, V., Thirion, B., Grisel, O., Blondel, M., Louppe, G., Prettenhofer, P., Weiss, R., et al. (2011). Scikit-learn: Machine Learning in Python. J. Mach. Learn. Res. *12*, 2825–2830. abs/1201.0490.
35. Benjamini, Y., and Hochberg, Y. (1995). Controlling the false discovery rate: A practical and powerful approach to multiple testing. J. R. Stat. Soc. Series B Stat. Methodol. *57*, 289–300.
36. Virtanen, P., Gommers, R., Oliphant, T.E., Haberland, M., Reddy, T., Cournapeau, D., Burovski, E., Peterson, P., Weckesser, W., Bright, J., et al. (2020). SciPy 1.0: fundamental algorithms for scientific computing in Python. Nat. Methods *17*, 261–272.
37. Seabold, S., and Perktold, J. (2010). Statsmodels: Econometric and statistical modeling with Python. In 9th Python in Science Conference, pp. 57–61.
38. Brennecke, P., Anders, S., Kim, J.K., Kołodziejczyk, A.A., Zhang, X., Proserpio, V., Baying, B., Benes, V., Teichmann, S.A., Marioni, J.C., and Heisler, M.G. (2013). Accounting for technical noise in single-cell RNA-seq experiments. Nat. Methods *10*, 1093–1095.
39. Osorio, D., Yu, X., Zhong, Y., Li, G., Yu, P., Serpedin, E., Huang, J.Z., and Cai, J.J. (2019). Single-Cell Expression Variability Implies Cell Function. Cells *9*, 14. https://doi.org/10.3390/cells9010014.
40. Cai, J.J. (2019). scGEAToolbox: a Matlab toolbox for single-cell RNA sequencing data analysis. Bioinformatics *36*, 1948–1949.
41. Love, M.I., Huber, W., and Anders, S. (2014). Moderated estimation of fold change and dispersion for RNA-seq data with DESeq2. Genome Biol. *15*, 550.
42. Yu, G., Wang, L.-G., Han, Y., and He, Q.-Y. (2012). clusterProfiler: an R package for comparing biological themes among gene clusters. OMICS *16*, 284–287.
43. Chen, S., Francioli, L.C., Goodrich, J.K., Collins, R.L., Kanai, M., Wang, Q., Alföldi, J., Watts, N.A., Vittal, C., Gauthier, L.D., et al. (2024). A genomic mutational constraint map using variation in 76,156 human genomes. Nature *625*, 92–100.
44. Kassambara, A. (2020). rstatix: Pipe-Friendly Framework for Basic Statistical Tests. R package version 0.7.2. https://rpkgs.datanovia.com/rstatix/.
45. Kuleshov, M.V., Jones, M.R., Rouillard, A.D., Fernandez, N.F., Duan, Q., Wang, Z., Koplev, S., Jenkins, S.L., Jagodnik, K.M., Lachmann, A., et al. (2016). Enrichr: a comprehensive gene set enrichment analysis web server 2016 update. Nucleic Acids Res. *44*, W90–W97.
46. Sloan, C.A., Chan, E.T., Davidson, J.M., Malladi, V.S., Strattan, J.S., Hitz, B.C., Gabdank, I., Narayanan, A.K., Ho, M., Lee, B.T., et al. (2016). ENCODE data at the ENCODE portal. Nucleic Acids Res. *44*, D726–D732.
47. Bernstein, B.E., Stamatoyannopoulos, J.A., Costello, J.F., Ren, B., Milosavljevic, A., Meissner, A., Kellis, M., Marra, M.A.,

Beaudet, A.L., Ecker, J.R., et al. (2010). The NIH Roadmap Epigenomics Mapping Consortium. Nat. Biotechnol. *28*, 1045–1048.
48. Kolde, R. (2018). pheatmap: Pretty Heatmaps. R package version 1.0.12. https://github.com/raivokolde/pheatmap.
49. Pedraza, J.M., and van Oudenaarden, A. (2005). Noise Propagation in Gene Networks. Science. *307(5717)*, 1965–1969.
50. Mojtahedi, M., Skupin, A., Zhou, J., Castaño, I.G., Leong-Quong, R.Y.Y., Chang, H., Trachana, K., Giuliani, A., and Huang, S. (2016). Cell fate decision as high-dimensional critical state transition. PLoS Biol. *14*, e2000640.
51. Bargaje, R., Trachana, K., Shelton, M.N., McGinnis, C.S., Zhou, J.X., Chadick, C., Cook, S., Cavanaugh, C., Huang, S., and Hood, L. (2017). Cell population structure prior to bifurcation predicts efficiency of directed differentiation in human induced pluripotent cells. Proc. Natl. Acad. Sci. USA *114*, 2271–2276.
52. Weick, J.P., Held, D.L., Bonadurer, G.F., 3rd, Doers, M.E., Liu, Y., Maguire, C., Clark, A., Knackert, J.A., Molinarolo, K., Musser, M., et al. (2013). Deficits in human trisomy 21 iPSCs and neurons. Proc. Natl. Acad. Sci. USA *110*, 9962–9967.
53. Ochiai, H., Hayashi, T., Umeda, M., Yoshimura, M., Harada, A., Shimizu, Y., Nakano, K., Saitoh, N., Liu, Z., Yamamoto, T., et al. (2020). Genome-wide kinetic properties of transcriptional bursting in mouse embryonic stem cells. Sci. Adv. *6*, eaaz6699.
54. Khetan, N., Zuckerman, B., Calia, G.P., Chen, X., Garcia Arceo, X., and Weinberger, L.S. (2024). Single-cell RNA sequencing algorithms underestimate changes in transcriptional noise compared to single-molecule RNA imaging. Cell Rep. Methods *4*, 100933.
55. Alemu, E.Y., Carl, J.W., Jr., Corrada Bravo, H., and Hannenhalli, S. (2014). Determinants of expression variability. Nucleic Acids Res. *42*, 3503–3514.
56. Wolf, S., Melo, D., Garske, K.M., Pallares, L.F., Lea, A.J., and Ayroles, J.F. (2023). Characterizing the landscape of gene expression variance in humans. PLoS Genet. *19*, e1010833.
57. Ochab-Marcinek, A., and Tabaka, M. (2010). Bimodal gene expression in noncooperative regulatory systems. Proc. Natl. Acad. Sci. USA *107*, 22096–22101.
58. Battich, N., Stoeger, T., and Pelkmans, L. (2015). Control of Transcript Variability in Single Mammalian Cells. Cell *163*, 1596–1610.
59. Bahar Halpern, K., Caspi, I., Lemze, D., Levy, M., Landen, S., Elinav, E., Ulitsky, I., and Itzkovitz, S. (2015). Nuclear Retention of mRNA in Mammalian Tissues. Cell Rep. *13*, 2653–2662.
60. Volteras, D., Shahrezaei, V., and Thomas, P. (2024). Global transcription regulation revealed from dynamical correlations in time-resolved single-cell RNA sequencing. Cell Syst. *15*, 694–708.e12.
61. Beaumont, H.J.E., Gallie, J., Kost, C., Ferguson, G.C., and Rainey, P.B. (2009). Experimental evolution of bet hedging. Nature *462*, 90–93.
62. Dueck, H., Eberwine, J., and Kim, J. (2016). Variation is function: Are single cell differences functionally important?: Testing the hypothesis that single cell variation is required for aggregate function. Bioessays *38*, 172–180.
63. Fraser, L.C.R., Dikdan, R.J., Dey, S., Singh, A., and Tyagi, S. (2021). Reduction in gene expression noise by targeted increase in accessibility at gene loci. Proc. Natl. Acad. Sci. USA *118*, e2018640118. https://doi.org/10.1073/pnas.2018640118.
64. Hansen, M.M.K., Desai, R.V., Simpson, M.L., and Weinberger, L.S. (2018). Cytoplasmic Amplification of Transcriptional Noise Generates Substantial Cell-to-Cell Variability. Cell Syst. *7*, 384–397.e6.
65. García-Blay, Ó., Hu, X., Wassermann, C.L., van Bokhoven, T., Struijs, F.M.B., and Hansen, M.M.K. (2025). Multimodal screen identifies noise-regulatory proteins. Dev. Cell *60*, 133–151. https://doi.org/10.1016/j.devcel.2024.09.015.
66. Hwang, S., Williams, J.F., Kneissig, M., Lioudyno, M., Rivera, I., Helguera, P., Busciglio, J., Storchova, Z., King, M.C., and Torres, E.M. (2019). Suppressing Aneuploidy-Associated Phenotypes Improves the Fitness of Trisomy 21 Cells. Cell Rep. *29*, 2473–2488.e5.
67. Klein, J.A., and Haydar, T.F. (2022). Neurodevelopment in Down syndrome: Concordance in humans and models. Front. Cell. Neurosci. *16*, 941855.
68. Dar, R.D., Hosmane, N.N., Arkin, M.R., Siliciano, R.F., and Weinberger, L.S. (2014). Screening for noise in gene expression identifies drug synergies. Science *344*, 1392–1396.
69. Karmiloff-Smith, A., Al-Janabi, T., D'Souza, H., Groet, J., Massand, E., Mok, K., Startin, C., Fisher, E., Hardy, J., Nizetic, D., et al. (2016). The importance of understanding individual differences in Down syndrome. F1000Res. *5*, F1000.Faculty.Rev-389. https://doi.org/10.12688/f1000research.7506.1.
70. Elowitz, M.B., Levine, A.J., Siggia, E.D., and Swain, P.S. (2002). Stochastic gene expression in a single cell. Science *297*, 1183–1186.
71. Qi, G., Strober, B.J., Popp, J.M., Keener, R., Ji, H., and Battle, A. (2023). Single-cell allele-specific expression analysis reveals dynamic and cell-type-specific regulatory effects. Nat. Commun. *14*, 6317.